Skin effect and losses in soft magnetic sheets: from low inductions to magnetic saturation

Skin Effect and Losses in Soft Magnetic Sheets: From Low Inductions to Magnetic Saturation

O. de la Barrière[1], E. Ferrara[2], A. Magni[2], A. Sola[2], C. Ragusa[3], C. Appino[2], and F. Fiorillo[2]

[1]Laboratoire SATIE, CNRS–ENS, 94320 Saclay, France
[2]Advanced Materials Metrology and Life Sciences, IstitutoNazionale di Ricerca-Metrologica-INRIM, 10135 Turin, Italy
[3]Energy Department, Politecnico di Torino, 10129 Turin, Italy

High frequencies are ubiquitous in present-day power applications: most electrical equipment, like rotating machines, are supplied by pulsewidth modulation (PWM) switching inverters, often working at tens or hundreds of kilohertz. PWM is responsible for minor cycles along the major hysteresis loop of the magnetic core, lasting a few microseconds. Such minor loops can cause deep skin effects, even if the thinnest today available laminations (0.1–0.2 mm thick sheets) are used. Common mode currents in the megahertz range, flowing from the electrical machine windings to the machine chassis through capacitive effects, can engender strong electromagnetic disturbances and bearing damages. A correct prediction of high-frequency phenomena is necessary, for example, for the accurate calculation of common mode filters, requiring a magnetic model of the laminated cores suited to high frequencies and low induction values and the ensuing dramatic skin effect. For power conversion applications, such as embedded planar transformers, the mandatory reduction of volume and cross-sectional area of the core, often made of high-permeability grain-oriented (HGO) sheets, imposes the increase of the conversion frequency from a few hundred hertz to several kilohertz and high peak induction values. The skin effect in this case is affected by the non-linear saturable magnetic response of the material and its treatment requires non-trivial experimental methods and modeling approaches. In this work, we discuss physically based modeling of the magnetization process and energy loss in magnetic sheets at high frequencies. We focus first on the low induction regimes occurring in thin non-oriented (NO) Fe–Si laminations. We consider then the case of high inductions, as encountered in power conversion devices using NO, HGO, and Fe–Co alloys, where non-linear models, possibly validated by magneto-optical observations of the domain wall (dw) dynamics, are developed and implemented.

Index Terms— **Fe–Co sheets, Fe–Si sheets, high frequencies, magnetic losses, skin effect.**

I. Introduction

STEEL laminations, such as the popular Fe–Si alloy, remain, after more than a century of constant improvements, the most used material in electrical engineering, thanks to a combination of excellent soft magnetic properties and the ease of stacking into the cores of electrical machines and transformers. Non-oriented (NO) sheets are employed when, like in electrical machines, isotropy is desired, whereas the high-permeability grain-oriented (HGO) alloys are the favorite material for power transformer cores.

In modern applications, the need to reduce the mass of the machines or the electronic supply system engenders a dramatic increase in the working frequencies, where the fundamental component can attain the range of several tens of kilohertz. At the same time, the use of high-frequency switching pulsewidth modulation (PWM) inverters (such as SiC or AsGa power transistors modules [1]) may cause harmonic spectra to broaden to hundreds of kilohertz. This associates with a surge of magnetic losses, which is countered in practice by the development of high-quality thin Fe–Si sheets, typically down to about 0.10 and 0.18 mm for the NO and HGO materials, respectively. Such a decrease partially mitigates the skin effect phenomena. It is shown, for example, that the threshold for them to appear is around $f = 400$ Hz for a 0.35 mm thick NO Fe-(3 wt.%)Si lamination, raising up to about 1 kHz in 0.20 mm thick sheets [2], far below, however, the requirements, in terms of peak induction B_p versus f response, of modern electrical engineering applications (see Fig. 1). The skin effect is a clear challenge in terms of modeling because the eddy current counterfield interacts with the material non-linearity. One has indeed to deal with quite a different scenario in the low induction domain, where a linear material response can approximately be invoked [3], and at high inductions, where non-linearity compounds with conditions leading to magnetic saturation [4].

In this article, we discuss the modeling of the magnetization process and energy loss in the presence of skin effect over a range of peak induction values. We shall distinguish between the previous two conditions, corresponding to low and medium-high induction values, respectively.

1) The low induction case (for example point 2 in Fig. 1), can be taken to correspond to B_p values lower than 0.1 T at frequencies of the order of a few hundred kilohertz. It is a condition attained in a high switching rate PWM supply, where the harmonics generate minor loops on the major hysteresis cycle [5]. Similar effects take place when common mode currents flow from the winding to the ground through capacitive effects [6].

2) We can conversely identify a high induction case with point 1 in Fig. 1. It is a condition commonly attained in embedded power transformers, where the core volume is reduced by adopting a working frequency of several kilohertz [7]. Thin

Manuscript received 27 March 2023; accepted 29 May 2023. Date of publication 8 June 2023; date of current version 24 October 2023. Corresponding author: O. de la Barrière (e-mail: olivier.de-la-barriere@satie.ens-cachan.fr).

Color versions of one or more figures in this article are available at https://doi.org/10.1109/TMAG.2023.3284421.

Digital Object Identifier 10.1109/TMAG.2023.3284421

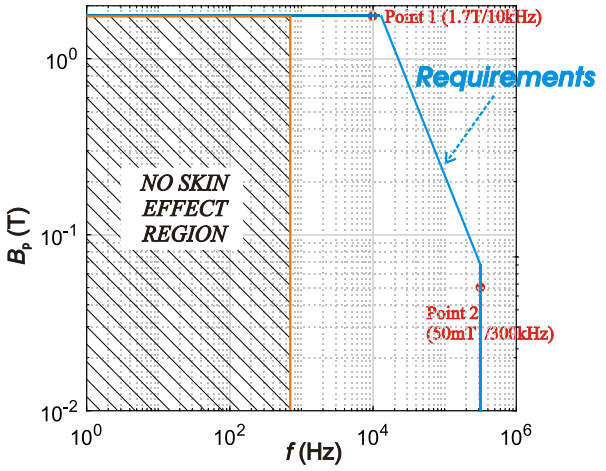

Fig. 1. Required B_p versus f working area in present-day electrical engineering applications.

HGO sheets are favored in these applications, in order to minimize the dynamic losses. We discuss in the following the case of 0.29 and 0.174 mm thick HGO steel sheets, where the treatment of the non-linear skin effect is lumped into a model for domain wall (dw) bowing and is associated with the results of dynamic magneto-optical observations.

3) Two-dimensional induction loci are commonly observed in the NO cores of rotating electrical machines [8], [9]. They are investigated in the literature by measurements and modeling, but the testing frequencies and the induction levels are generally lower (up to a few hundred hertz) than the ones observed in the cores of modern electrical machines. The kilohertz range is, for example, encountered in transportation or energy storage actuators [10].

In this article, research results concerning 2-D induction loci in NO laminations up to the kilohertz range are presented. The skin effect under rotating inductions is put in evidence and physically interpreted.

II. Literature Survey

The increasing share of high-frequency applications in electrical engineering has revived interest in the ancient research topic of the skin effect in magnetic laminations. The goal is to predict the hysteresis cycle, or at least the energy loss, in soft magnetic sheets at high frequencies. It is an objective pursued in most cases by empirical-phenomenological approaches, where a certain amount of experimental data is translated into ad hoc parameters, to be generally refreshed any time the working conditions (peak polarization value, induction waveform, lamination thickness, etc.) are modified. Physically based methods, aiming at a general assessment of the phenomena, rely on the solution of the electromagnetic diffusion equation governing the high-frequency magnetization reversal. The crucial point here is one of defining and treating the appropriate magnetic constitutive law of the material, up to the approach to saturation.

A. Phenomenological Skin Effect Models

The phenomenological approaches have the advantage of being computationally fast, but they require an important amount of experimental data. Most of them are either based on suitably modified Steinmetz laws or manipulations of the loss separation formulas. It has been suggested, for example, to change the power law of the classical loss component to extend the frequency of the loss separation formula [11] or to express Maxwell's diffusion equation by adopting a fractional induction derivative [12]. Coefficients for the loss components variable with peak induction and frequency have also been proposed [13], [14]. Note that the nonuniform profile of the magnetization across the sheet thickness imposed by the skin effect associates with a value of the quasi-static (hysteresis) loss different with respect to the case of uniform profile. A formulation for the eddy current losses, derived from the statistical theory of losses (STL) [15], is provided in [16], where, to account for the skin effect, the standard expressions for the classical and excess loss components are empirically multiplied by logarithmic functions of frequency. An extension of the loss-surface (LS) hysteresis model to high frequencies has also been proposed [17], where new formulations for the dynamic losses are provided. Other authors have coupled the analytical solution of Maxwell's diffusion equation with the inverse static Jiles–Atherton (JA) model in order to predict the hysteresis loop at medium frequencies and moderate flux penetration [18].

B. Linear Skin Effect Models

Analytical solutions for a linear material (a material with constant permeability) are well-known [19], and can be expressed in terms of hyperbolic functions. The main problem consists in treating the non-linear material behavior by approximating it to a linear one. It is proposed in [20] and [21] to fit the measured loss over an extended frequency range by formulating the classical energy loss in the presence of skin effect as

$$W_{\text{class}} = bB_p^2 f^{1/2} \frac{\sinh\left(d\sqrt{f}\right) - \sin\left(d\sqrt{f}\right)}{\cosh\left(d\sqrt{f}\right) - \cos\left(d\sqrt{f}\right)} \tag{1}$$

where d is the lamination thickness, B_p is the peak induction value, f is the working frequency, and b is a B_p-dependent fitting parameter. The hysteresis and excess loss components are assumed unaffected by the skin effect, a strong simplification. A similar approach is followed in [22].

The mathematical works of [23], [24], and [25] are based on the linear solution of the diffusion equation in a single lamination, so as to provide a homogenized complex (or time-depending) permeability to the finite element (FEM) design of electrical machines, taking into account the loss due to eddy currents. Such works have been extended in [26] to the case of a stack of laminations with spurious contacts due to core assemblage.

The linear diffusion equation has been solved in [27] and [28] by assuming, for imposed macroscopic peak induction B_p (the average across the sheet thickness) the permeability B_p/H_p measured on a quasi-static loop. The loss associated with the small minor hysteresis loops taken along a major hysteresis loop is considered in [29]. Because of the involved small induction swing, the use of a linear model, where the

measured reversible permeability is retained for the calculation, is justified.

C. Non-Linear Skin Effect Models

The diffusion equation solved in the linear approximation leads to unrealistic peak induction values in the cross-sectional region close to the sheet surface. Consequently, the actual non-linear saturating $B(H)$ characteristic of the material must be taken into account. This is done, for example, in [30], where a homogenization method is applied to the $B(H)$ curve, assumed to be single-valued, and a pseudo-linear approach has been proposed using a differential reluctivity tensor.

For modeling high-frequency losses in NO materials, Dupre et al. [31] have solved the non-linear hysteretic diffusion equation using the dynamic Preisach model (DPM) as the local constitutive law, extending an early derivation based on the use of the static Preisach model (SPM) [32]. A similar approach has been followed by Engdahl [33], [34], using static and dynamic play–stop hysteresis models. There is a heavy computational burden associated with these dynamic models, which may require a special convergence procedure (such as the fixed-point method). Moreover, such an approach is only valid for NO materials, in which the grain size is small, and the domain structure is dense. In any case, satisfying results are obtained in terms of loss prediction, as shown in the so-called 1-D–2-D model [35]. The diffusion equation is solved in one dimension, along the direction perpendicular to the sheet plane and the constitutive equation is used to model a 2-D problem in the plane [36]. This approach has been further extended to 2-D induction loci, using a Mayergoyz vector hysteresis model as a local $B(H)$ constitutive law [37]. The specific interpretation of reduced flux penetration in terms of dw bowing was highlighted by Zirka et al. [38].

The problem of magnetic dissipation at very high frequencies, up to hundreds of MHz, has been investigated by Magni et al. [39], [40], [41] in amorphous and nanocrystalline ribbons, 10–20 μm thick. The modeling is based on the solution of the 1-D Maxwell's diffusion equation in transversally annealed ring samples, where the dominant process is made of coherent magnetization rotations. The constitutive equation is in this case obtained in terms of complex permeability as the solution of the Landau–Lifshitz–Gilbert equation. In the small signal approximation, an analytical expression for the energy loss can eventually be derived [42].

III. Small-Amplitude Hysteresis Cycles

Small-amplitude hysteresis cycles arise in numerous applications (e.g., fast minor cycles in PWM or magnetic effect of common mode currents flowing in electrical machines supplied by PWM inverters). We discuss the loss calculation in this case by considering first the frequencies in the kHz range, with an application to PWM loss prediction. In the second part, we extend the results to higher frequencies.

A. Small Cycles up to 10 kHz

A 0.20 mm thick Fe-(3.2 wt.%) Si sheets (in which the skin effect may be significant beyond about 1 kHz) have been investigated up to 10 kHz, for peak polarization value $J_p = 200$ mT (peak induction B_p and polarization J_p are synonymous in this case) [3]. The permeability μ, assumed to be a real quantity, is identified at low frequency as the constitutive equation and the classical loss in the sheet of thickness d is calculated using the equation for the linear skin effect

$$W_{\text{class}}(B_p, f) = \frac{\pi^2}{6}\sigma d^2 B_p^2 f \cdot F_{\text{class}} \tag{2}$$

where $F_{\text{class}} = (3/d/\delta) \cdot (\sinh(d/\delta) - \sin(d/\delta)/\cosh(d/\delta) - \cos(d/\delta))$, $\delta = 1/(\pi\mu\sigma f)^{1/2}$ is the skin depth and σ is the electrical conductivity. Equation (2) is justified by the low J_p value ($J_p = J_s/10$, with J_s the saturation polarization), such that the predicted polarization at the sheet surface is always below J_s at 10 kHz. W_{class} calculated by (2) in these thin Fe–Si laminations is validated by the performed loss separation procedure [3], where the excess loss, obtained by subtracting the classical loss (2) and the hysteresis loss W_{hyst} to the measured loss $W(f)$, depends on the square root of the frequency, as predicted by the STL theory [15]. The conclusions are listed as follows:

1) The skin effect can be quite easily accounted for using linear formulae at low induction values because the peak polarization value at the lamination surface remains, at the frequencies of interest, reasonably limited.

2) The excess loss still depends on the square root of frequency in the skin-effect region. It depends, in particular, on the mean induction value, even if the induction profile is nonuniform across the sample thickness.

We also remark that at the involved low J_p values the quasi-static response of the material obeys the Rayleigh law and one can, in any case, approximate the actual hysteresis loop with an elliptical loop, the higher the frequency, the better the approximation. We can therefore specialize the model by taking the complex permeability $\underline{\mu} = \mu' - j\mu''$, identified with the dc elliptical loop, as the constitutive equation of the material [5]. The classical loss is therefore obtained according to the expression

$$W_{\text{class}}(B_p, f) = \frac{\pi}{2}\frac{B_p^2}{|\underline{\mu}|} \cdot \frac{(\lambda' - \lambda'')\sinh(\lambda' - \lambda'') - (\lambda' + \lambda'')\sin(\lambda' + \lambda'')}{(\lambda' - \lambda'')\cosh(\lambda' - \lambda'') - (\lambda' + \lambda'')\cos(\lambda' + \lambda'')} \tag{3}$$

where

$$\lambda = \lambda' + \iota\lambda'' = \sqrt{\frac{2\pi f\sigma|\underline{\mu}|d^2}{2}} \cdot \left(\sqrt{\frac{1 + \mu'/|\underline{\mu}|}{2}} - \iota \cdot \sqrt{\frac{1 - \mu'/|\underline{\mu}|}{2}}\right). \tag{4}$$

The excess loss is assumed to depend on the mean peak induction J_p (averaged across the sheet thickness) and is calculated with the usual STL formulation [15]. It is remarked,

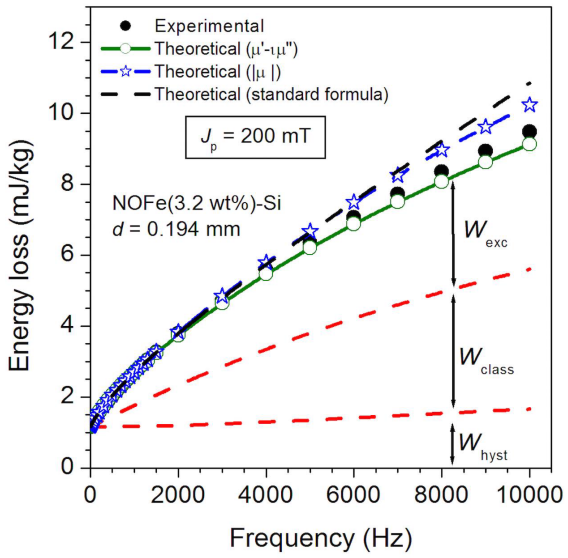

Fig. 2. Energy loss $W(f)$ measured at $J_p = 200$ mT in the 0.194 mm thick NO Fe–Si sheet is compared with different theoretical predictions up to 10 kHz. The standard formula disregards the skin effect. The solid line (open circles) and the loss components $W_{\text{hyst}}(f)$ and $W_{\text{exc}}(f)$, are calculated assuming the dc complex permeability $\underline{\mu} = \mu' - j\mu''$ as the material constitutive equation at low J_p values. (Adapted from [5].)

instead, that the hysteresis loss W_{hyst}, by virtue of its local nature (Barkhausen jumps), depends instead on the J_p profile $j_p(x)$, with x ranging between $\pm d/2$. Consequently, it becomes an increasing function of frequency, according to the following equation:

$$W_{\text{hyst}}(J_p, f) = \frac{1}{d}\int_{-\frac{d}{2}}^{\frac{d}{2}} k j_p^{\alpha}(x)dx \tag{5}$$

where we introduce the experimental quasi-static power law dependence $W_{\text{hyst}}(J_p) = kJ_p^{\alpha}$. A clear improvement in terms of loss prediction capability is observed in Fig. 2 by assuming the complex permeability as the constitutive equation of the material at low J_p values.

This model has been successfully applied in [5] to predict the loss due to fast minor cycles in PWM induction waveforms.

B. Toward Very High Frequencies

1) Classical Loss W_{class}: The previous linear simplification falls short of experiments on increasing the frequency to hundreds of kilohertz because this engenders an extreme variation of $j_p(x)$ and a strongly non-linear regime. To overcome this problem, we express the diffusion equation across the thickness of the indefinitely wide sheet

$$\begin{cases} \frac{\partial^2 h}{\partial x^2} - \sigma \frac{\partial b}{\partial t} = 0 \\ \frac{\partial h}{\partial x}\Big|_{x=\pm d/2} = \sigma \frac{d}{2}\frac{dB}{dt} \end{cases} \tag{6}$$

where the functions $h(x)$ and $b(x)$ are respectively the local magnetic field and inductions, and B is the mean induction across the sheet thickness. Equation (6) is solved by identifying the $b(h)$ constitutive law with the normal magnetization curve, the locus of the tip points of the symmetric quasi-static minor loops, as shown for a 0.20 mm thick Fe-(3.2 wt.%)Si sheet in Fig. 3. The non-linearity is treated in this case by means of a fixed-point procedure [31].

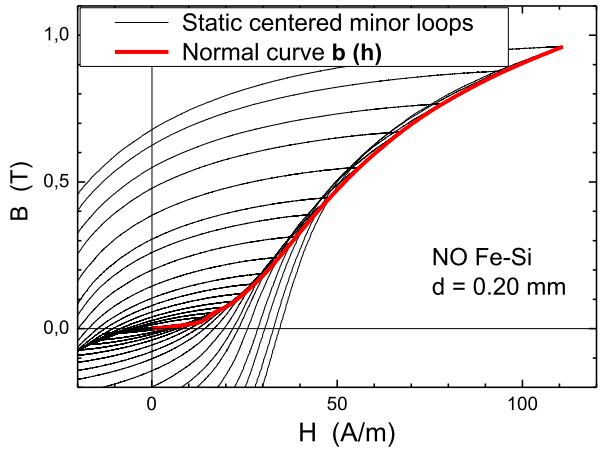

Fig. 3. Normal magnetization curve of the NO 0.20 mm thick Fe-(3.2 wt.%)Si sheet. It is obtained as the locus of the tip points of an ordered sequence of symmetric quasi-static minor loops. This curve is taken as a simplified magnetic constitutive equation $b(h)$ of the material.

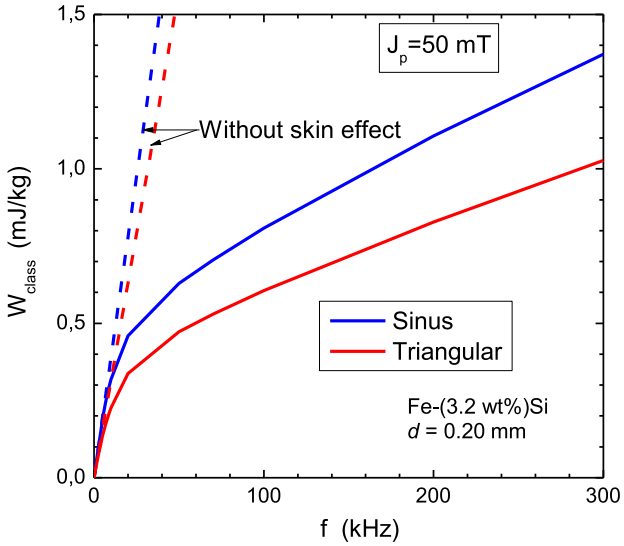

Fig. 4. Classical loss W_{class} versus frequency up to $f = 300$ kHz calculated for a thickness-averaged peak polarization $J_p = 50$ mT (sinusoidal and triangular) in a NO 0.20 mm thick Fe-(3.2 wt.%)Si sheet.

The integration across the sheet thickness of the local power dissipation j^2/σ, where $j(x) = dh/dx$ is the current density, provides the classical loss component $W_{\text{class}}(f)$. This quantity is represented in Fig. 4, where the calculations are made upon the broad frequency range dc–300 kHz for sinusoidal and triangular polarization waveforms having the same peak value $J_p = 50$ mT. It is noted the change of slope of $W_{\text{class}}(f)$ occurs on overcoming $f = 10$ kHz, concurrent with the appearance of a strong skin effect.

The prominent role of the skin effect is apparent in the calculated behavior of the peak value b_p of the local induction $b(x,t)$ as a function of x shown in Fig. 5 for $f = 300$ kHz. The maximum $b_p(d/2)$ at the sheet surface is about 0.8 T, i.e., 16 times higher than the mean peak value $J_p = 50$ mT. Because of the increase of the permeability on the

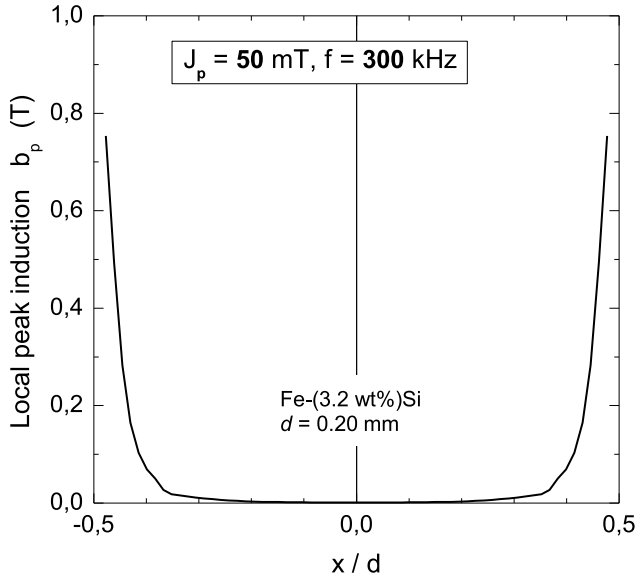

Fig. 5. Peak induction $b_p(x)$ versus depth in the $d = 0.20$ mm thick Fe-(3.2 wt.%)Si sheet at $f = 300$ kHz for a thickness-averaged peak polarization $J_p = 50$ mT (sinusoidal case).

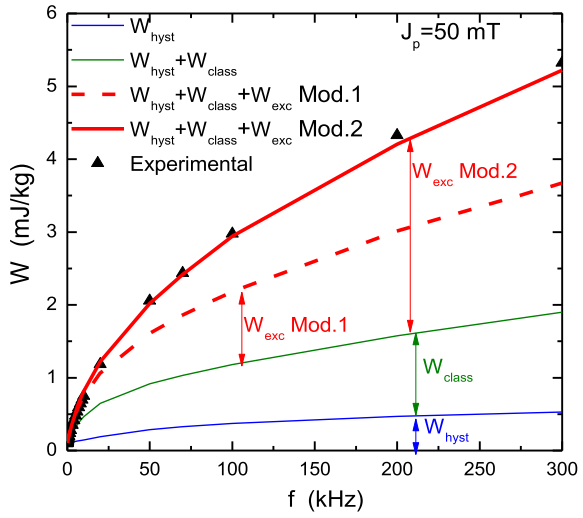

Fig. 7. Energy loss $W(f)$ at $J_p = 50$ mT (sinusoidal case), measured up to $f = 300$ kHz (symbols) is compared with the theoretical prediction $W(f) = W_{\text{hyst}}(f) + W_{\text{clas}}(f) + W_{\text{exc}}(f)$. The excess loss has been computed using $V_o(J_p)$ (Model 1), and using $V_o(j_{\text{pM}})$ (Model 2).

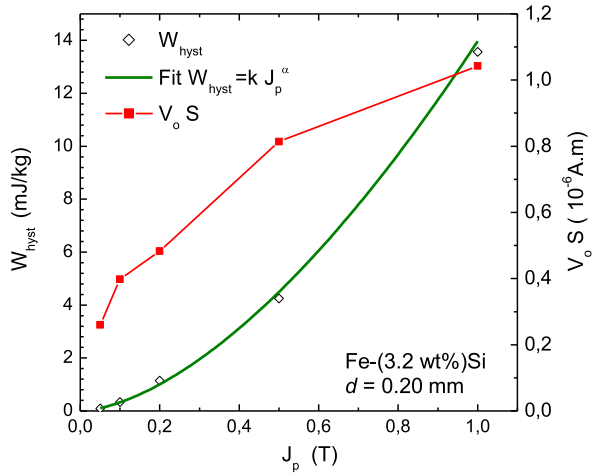

Fig. 6. Dependence of the hysteresis loss W_{hyst} and the statistical parameter V_o (more precisely $V_o \cdot S$, where S is the sample cross-sectional area) at low frequencies as a function of the peak induction J_p. These quantities are derived from the loss separation procedure made up to 1 kHz according to the STL.

magnetization curve observed in this b_p range (see Fig. 3), the skin effect is enhanced with respect to the linear case, where the diffusion (6) is solved for constant magnetic permeability.

2) Excess W_{exc} and Hysteresis W_{hyst} Components: We start by making the loss decomposition in the Fe–Si sheet up to frequencies for which the skin effect can still be disregarded, i.e., up to 1 kHz for the previous 0.20 mm thick sample. The hysteresis W_{hyst} and excess $W_{\text{exc}}(f)$ loss contributions are in this case identified according to the standard approach by the STL [15]. The so-obtained hysteresis loss $W_{\text{hyst}}(J_p)$ and the basic statistical parameter $V_o(J_p)$ [14] are shown in Fig. 6. It is observed that the hysteresis loss depends on J_p according to the power law $W_{\text{hyst}}(J_p) = k.\ J_p^{\alpha}$, with $\alpha = 1.64$. It is then calculated locally using (5) and the obtained peak induction profile $b_p(x)$ (see Fig. 5). By evolving together with the $b_p(x)$ profile, the hysteresis loss is bound to increase with frequency.

Let us assume that the excess loss can be expressed in terms of the measured (thickness-averaged) polarization J_p, even in the presence of skin effect. With sinusoidal flux, we write, according to the formulation provided by the STL [15]

$$W_{\text{exc}}(J_p, f) = 8.76 \cdot \sqrt{\sigma G S V_o} J_p^{1.5} \sqrt{f}\,(\text{J/m}^3) \qquad (7)$$

where $G = 0.1356$, S is the sample cross-sectional area, and V_o is the previously introduced and shown in Fig. 6 J_p-dependent statistical parameter, a measure of the local coercive field and its distribution. Two simplifications involving the parameter V_o can be made in the calculations.

1) Model 1. The function V_o is associated with the measured mean polarization J_p, as previously assumed. This is the simplest alternative, already validated up to 10 kHz.

2) Model 2. With the increase of the magnetizing frequency and the rise of an extreme peak induction profile $b_p(x)$, like the one shown in Fig. 5, Model 1 involves too a drastic approximation. Under such a deep $b_p(x)$ profile, and the magnetization taking appreciable values only close to the sheet surface, we might actually assume for the parameter V_o the value $V_o(j_{\text{pM}})$, where $j_{\text{pM}} \cong b_{\text{pM}}$ is the maximum value of the local peak polarization attained at a given frequency across the sheet thickness. According to the STL, in making the prediction of the excess loss we need to consider the statistical properties of the magnetic objects, defined as the mesoscopic regions (typically the grains in a polycrystalline material) where the elementary dw processes are tightly correlated [15]. By assuming that $V_o \equiv V_o(j_{\text{pM}})$, we take into account the fact that, with a profile like the one shown in Fig. 5, the activation of the magnetic objects by the changing field chiefly occurs in a narrow region close to the sheet surface, where the magnetization process is concentrated.

Fig. 7 shows an example of loss decomposition in the 0.20 mm Fe-(3.2 wt.%)Si sheet up to $f = 300$ kHz at $J_p = 50$ mT. $W_{\text{hyst}}(f)$ and $W_{\text{clas}}(f)$ are obtained according to (5) and (4), respectively, while $W_{\text{exc}}(f)$ is calculated following

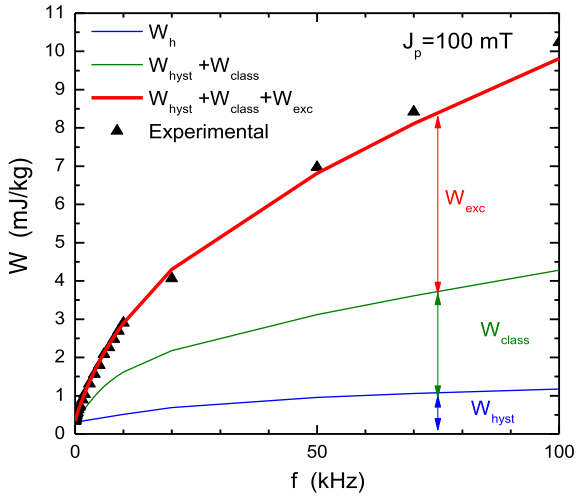

Fig. 8. Energy loss $W(f)$ at $J_p = 100$ mT (sinusoidal case), measured up to $f = 100$ kHz (symbols) is compared with the theoretical prediction $W(f) = W_{\text{hyst}}(f) + W_{\text{clas}}(f) + W_{\text{exc}}(f)$ (Model 2).

either Model 1 or Model 2. The theoretical behavior of the total loss $W(f) = W_{\text{hyst}}(f) + W_{\text{clas}}(f) + W_{\text{exc}}(f)$ is then represented by the dashed and solid curves following Model 1 and Model 2, respectively. The two models provide the same predictions at relatively low frequencies, up to about 20 kHz, to diverge progressively on increasing f, where Model 2 provides good fitting of the experimental results up to a maximum experimental frequency of 300 kHz. We shall retain Model 2 for further calculations. To note the non-linear increase of the calculated components $W_{\text{hyst}}(f)$ and $W_{\text{class}}(f)$, as well as the persisting conspicuous role of $W_{\text{exc}}(f)$ at high frequencies, favored by the skin effect.

The measurements have been repeated at $J_p = 100$ mT, by keeping, because of power constraints, the upper frequency at 100 kHz. The experimental $W(f)$ and its prediction, obtained as the sum of the calculated hysteresis, classical, and excess components, are provided in Fig. 8. Again, the theoretical formulation making use of Model 2 appears to provide good agreement with the experimental energy loss behavior across the whole broad frequency range.

IV. Loss at High Inductions and High Frequencies

At high inductions (i.e., depending on the alloy, beyond about 0.5 T up to magnetic saturation), the linear approach is too far from a reasonable description of the magnetic constitutive law of the material and it would lead to unrealistic induction levels close to and at the sample surface. Consequently, we must resort to non-linear $b(h)$ modeling of the material magnetic constitutive law. A distinction is made between NO and HGO materials.

A. NO Fe–Si Sheets

The high-frequency losses of the NO Fe–Si alloys have been treated in [31] by assuming the magnetic constitutive law resulting from the application of the DPM. Since NO sheets have small grains and domains, it is reasonable to assume that each FEM (or elementary slice of the material) used to discretize the diffusion equation is representative of the statistics of magnetic objects on which the Preisach modeling is based.

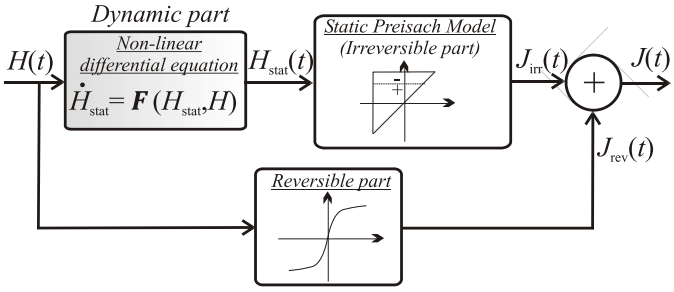

Fig. 9. Computational scheme of the simplified approach to the diffusion equation and solution using a dynamical constitutive law. (Adapted from [4].)

The drawback of such a procedure lies in its complexity and the computation time required to achieve convergence. This is mostly due to the cumbersome implementation required by the DPM and the related discretization of the Preisach plane. It was thus suggested to resort to the SPM, which does not require, using the Everett formalism, a double integral computation for each time step [43]. Lacking the dynamical contribution, this approach leads, however, to relatively crude predictions [32]. Consequently, a procedure was realized, where the diffusion equation is solved with the use of a dynamical constitutive law requiring a reduced computational burden, which is comparable to the one associated with the SPM [4], [44]. This model is schematically illustrated in Fig. 9.

We start from the concept of static field H_{stat}, defined as the field that would give the SPM the same irreversible polarization J_{irr} as the dynamic field H of the DPM. The operator F in Fig. 9 represents a non-linear differential equation linking the two fields, which can be numerically solved with a negligible computation time. As demonstrated in [4], the following differential equation relates H_{stat} with the known H value (k_d is the constant introduced in the DPM theory [31]):

$$\dot{H}_{\text{stat}} = \text{sign}[H(t) - H_{\text{stat}}(t)]\frac{9}{16}k_d[H(t) - H_{\text{stat}}(t)]^2. \quad (8)$$

Once the field H_{stat} is known, the computational scheme of Fig. 9 shows that the SPM, faster and computationally more efficient than the DPM, can be used to relate $H(t)$ and $J(t)$ at any frequency.

Examples of loss prediction in 0.20 mm thick Fe–Si and Fe–Co–V samples by the simplified approach illustrated in Fig. 9 and (8) are provided in Fig. 10 in comparison with the results obtained applying the conventional DPM-based approach [31].

The predicted local induction profiles $b_p(x)$ in the Fe–Co alloy at 10 kHz for peak polarizations $J_p = 0.5$ and 1.7 T are given in Fig. 11. Again, the DPM and the SPM-based models provide very close results. It is observed how for $J_p = 1.7$ T the material magnetically saturates on approaching the sheet surface.

B. HGO Sheets

HGO laminations are of importance for transformers cores, which, as previously mentioned, are brought to kilohertz working frequencies when high power densities are required. The predicting approach previously employed for NO laminations,

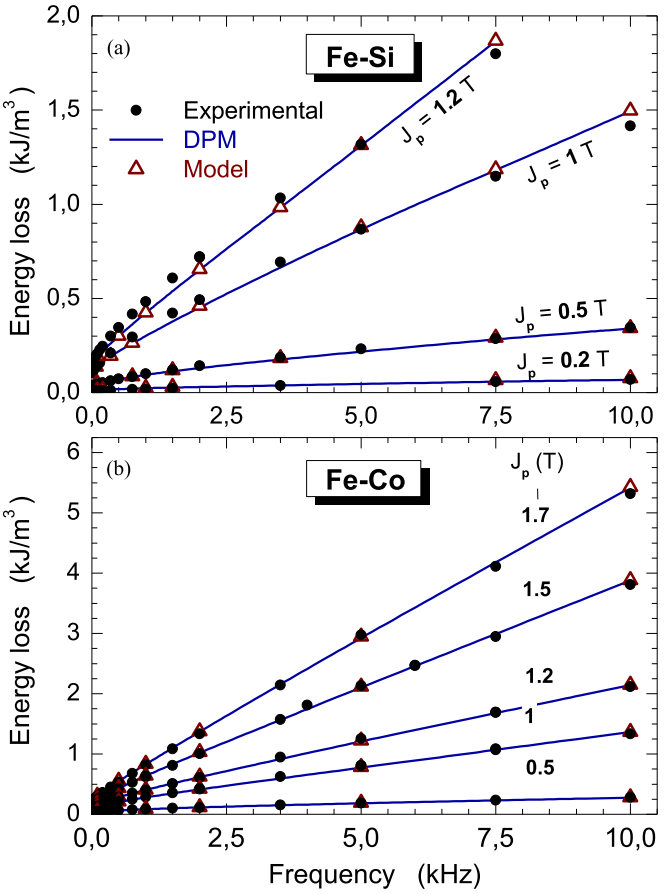

Fig. 10. Energy loss versus frequency at different polarization values J_p (full symbols) in 0.20 mm thick (a) NO Fe–Si and (b) Fe–Co Vacoflux sheets. Solid line: prediction by the DPM. Open triangle: prediction by the SPM-based. (Adapted from [4].)

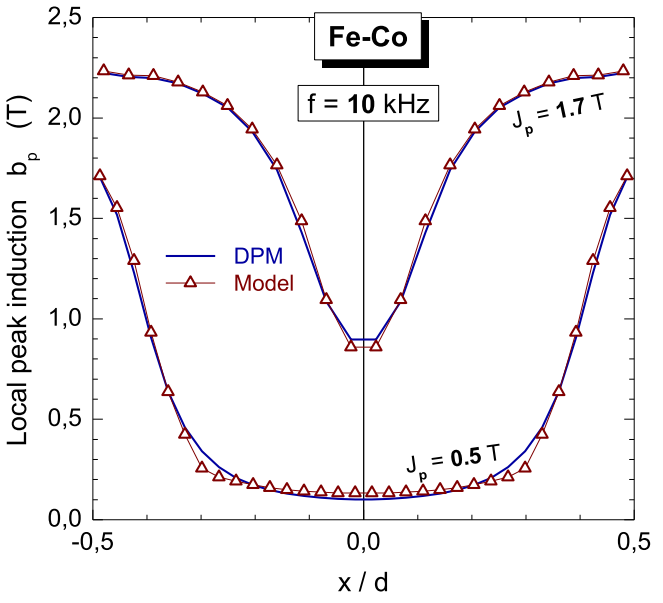

Fig. 11. Calculated profile of the local peak induction value $b_p(x)$ across the lamination thickness in 0.20 mm Fe–Co laminations at 10 kHz. (Adapted from [4].)

cannot be directly translated to the behavior of HGO sheets, because these have large grains, wide domains, and extended walls, running through the sheet thickness. Discretization of

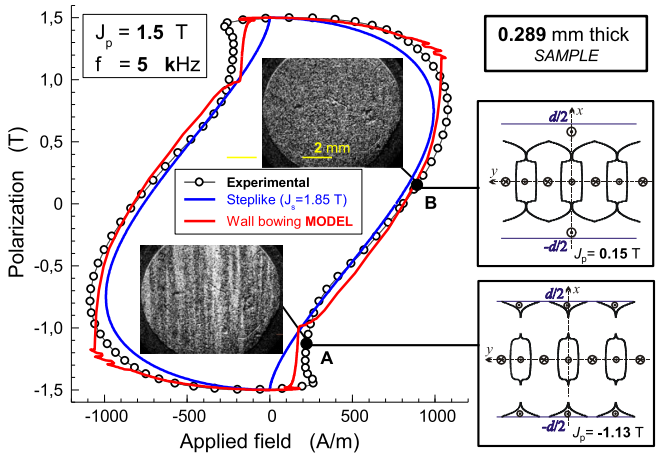

Fig. 12. Experimental cycle taken between ±1.5 T at 5 kHz on a 0.289 mm thick HGO sheet (symbols) and cycle predicted by the dw bowing numerical model. The dw patterns theoretically envisaged to occur at two different times A and B along the semi-cycle (right-hand side) are compared with the correspondingly obtained surface magneto-optical images. The appearance of a horizontal front is contemplated by the calculations. The hysteresis loop predicted for the ideal case of step-like constitutive magnetization curve is also shown.

the cross section along this direction and application of the hysteresis law to each FEM would be hardly justified. We can nevertheless still rely, even in the presence of skin effect, on the concept of loss decomposition [14], [45]. The key point becomes one of looking at and possibly predicting the evolution with a frequency of the discrete pattern of the [1] directed antiparallel domains and the cross-sectional profile of their 180° dws. Such an evolution can be followed by Kerr observations of the wall dynamics.

Recent experiments have been carried out on HGO sheets of thickness 0.289 and 0.174 mm, combining Kerr and fluxmetric measurements, up to 10 kHz [45], [46]. At sufficiently high J_p values and frequencies, merging of the walls at the sheet surface is observed, an effect having an obvious origin in the severe dw bowing imposed by the eddy currents. With the aid of a numerical simulation of the motion of a regular array of 180° dws, wall bowing and merging is predicted and the related hysteresis loop is calculated [46]. Fig. 12 provides an illustrative example of cross-sectional patterns of the walls predicted to occur at two different times (A and B) along a cycle performed between $J_p = \pm 1.5$ T at 5 kHz on the 0.289 mm thick lamination. The calculated patterns consistently compare with the magneto-optical imaging of the surface domain structure. In addition, the calculated hysteresis loop is close to the experimental one.

The predicted domain patterns point to a progressive evolution of the magnetization process from the low-frequency low-induction back-and-forth motion of the 180° dws to the motion of reversal fronts proceeding inward from the opposite sheet surfaces. It is reminding of the reversal predicted to occur in an idealized material endowed with a step-like constitutive magnetization curve $J(H) = J_S \cdot \mathrm{sign}(H)$ (see Fig. 13) [47].

For this limiting case, the analytical expression for the loss, now reduced to a classical formulation, is obtained as [47]

$$W_{\mathrm{class}}^{(\mathrm{STEPLIKE})}(B_p, f) = \frac{3}{2}\frac{B_p}{J_S}\frac{\pi^2}{6}\sigma d^2 B_p^2 f. \qquad (9)$$

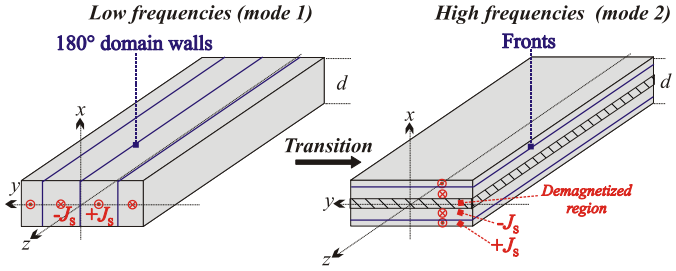

Fig. 13. Transition to the front model at high frequencies.

It amounts to the classical loss calculated in the absence of skin effect multiplied by the ratio $3/2 \cdot B_p/J_S$.

The ideal steplike cycle, represented in blue in Fig. 12, is close to the experimental cycle (green symbols), but for the extra area appearing at the reversal points. In these regions (e.g., point A in Fig. 12), dw activity associated with domain nucleation occurs, before the formation of the horizontal front. This activity gives then rise to an extra loss (i.e., an excess loss), congruent with the low-frequency definition of the excess loss, the contribution generated by the eddy currents enwrapping the moving dws [47, pp. 410]. This excess contribution, visibly taking place at the reversal points, is quite correctly predicted by the numerical wall-bowing model (red cycle in Fig. 12), but it will inevitably disappear under a further increase in frequency.

The loss analysis in the presence of skin effect can therefore be summarized according to the following points:

1) The classical loss $W_{\text{class}}(f)$ can be consistently defined, in accordance with the conventional low-frequency definition, as the loss obtained through the solution of Maxwell's diffusion equation with the normal curve taken as the $J(H)$ constitutive law [45].

2) The hysteresis loss $W_{\text{hyst}}(f)$ is obtained as the volume integration of the microscopically localized quasi-static loss. At any point of the sheet cross section, it is well approximated by a power law dependence on the local $j_p(x)$ value and is macroscopically defined according to (5). It is noted that $W_{\text{hyst}}(f)$ vanishingly contributes to the high-frequency loss in the HGO sheets.

3) The excess loss $W_{\text{exc}}(f)$ is obtained by subtracting $W_{\text{hyst}}(f)$ and $W_{\text{class}}(f)$ to the measured loss $W(f)$. It is shown to follow an $f^{1/2}$ dependence on a frequency below the skin effect region. It tends to vanish, together with $W_{\text{hyst}}(f)$, in the upper right corner (J_p, f). This is understood, looking at the results shown in Fig. 12, due to the evolution of the dw processes toward a reversal front mechanism.

Loss decomposition at $J_p = 1.7$ T in two different HGO sheets (0.29 and 0.174 mm thick) is provided in Fig. 14. It is observed that the measured $W(f)$ tends to coincide, beyond a few kilohertz, with the classical loss $W_{\text{class}}(f)$, calculated according to the previous discussion, to eventually approach the value given by (9). These results show the users the great benefit of choosing a thinner HGO lamination. They further show how the interaction between the electromagnetic diffusion process and the material non-linearity leads to a classical regime at high frequencies, via a disruptive evolution of domain structure and dw dynamics.

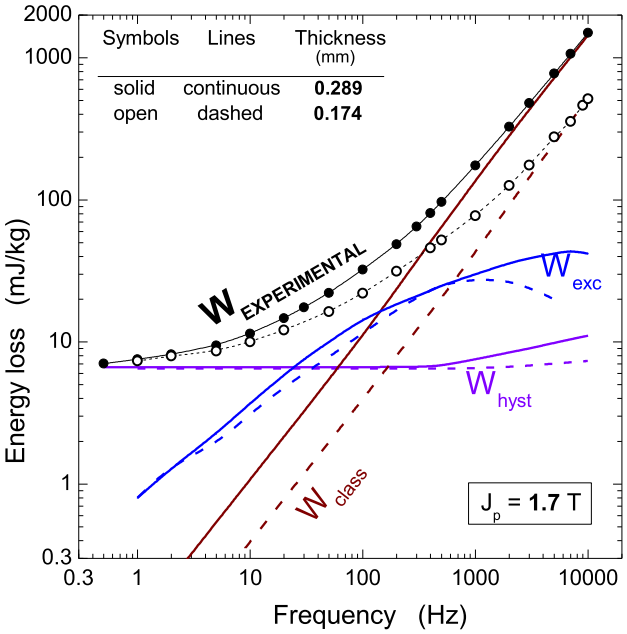

Fig. 14. Loss separation in two HGO steel sheets (0.29 and 0.174 mm thick) for $J_p = 1.7$ T. The classical loss $W_{\text{class}}(f)$ has been calculated by identifying the magnetic constitutive equation of the material with the normal magnetization curve in Maxwell's diffusion equation. The excess $W_{\text{exc}}(f)$ and hysteresis $W_{\text{hyst}}(f)$ loss components become negligible beyond a few kilohertz.

V. Two-Dimensional Magnetization at High Frequencies

Modern high-speed electrical machines are commonly endowed with fundamental frequencies in the kilohertz range. They are also affected by 2-D fluxes, whose response to J_p and f is largely at variance with respect to the alternating behavior. Since loss models for arbitrary 2-D induction loci usually require circular induction loci measurements as a prerequisite [48], it is necessary to apprehend and model circular induction loci in the kilohertz range for a meaningful treatment of the problem.

A. Thick Low-Carbon Steel Sheet

Most rotating induction measurements require substantial exciting power and are generally restricted to a few hundred hertz. To reach the kilohertz range at reasonably high J_p values (e.g., $J_p > 1.0$ T) a specific 2-D magnetizer, based on a digitally controlled three-phase supply and wattmetric setup was developed, as discussed in detail in [49]. The interest in the response to rotational fields of low-carbon steels brought at high induction values relates to their still pervasive applications in rotating machines. Because of their significant conductivity and thickness, low-carbon steel laminations are prone to the skin effect already at relatively low frequencies. We discuss then the rotational energy loss W_{rot} measurements performed on 0.64 mm thick samples (resistivity $\rho = 12.51 \cdot 10^{-8}$ Ω·m, density $\delta = 7850$ kg/m^3) under circular polarization loci. Fig. 15 shows the J_p dependence of the rotational loss measured up to 1.7 T and 1 kHz [50].

We might at first calculate the classical loss disregarding the skin effect, according to the standard equation

$$W_{\text{class}}^{(\text{ROT})}(B_p, f) = \frac{\pi^2}{3} \cdot \frac{d^2 B_p^2}{\rho} f \quad [\text{J/m}^3]. \tag{10}$$

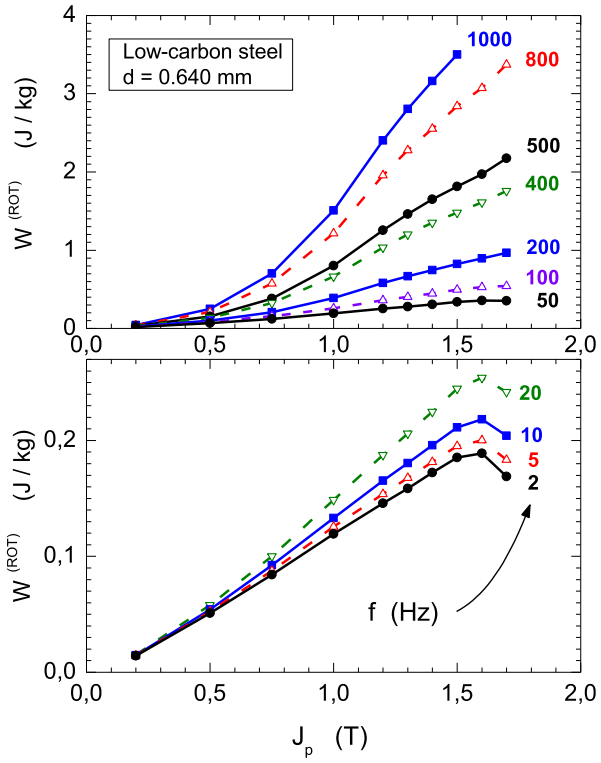

Fig. 15. Rotational energy loss versus circular polarization J_p measured in a 0.640 mm thick low-carbon steel sheet in the frequency range 2 Hz to 1 kHz [50].

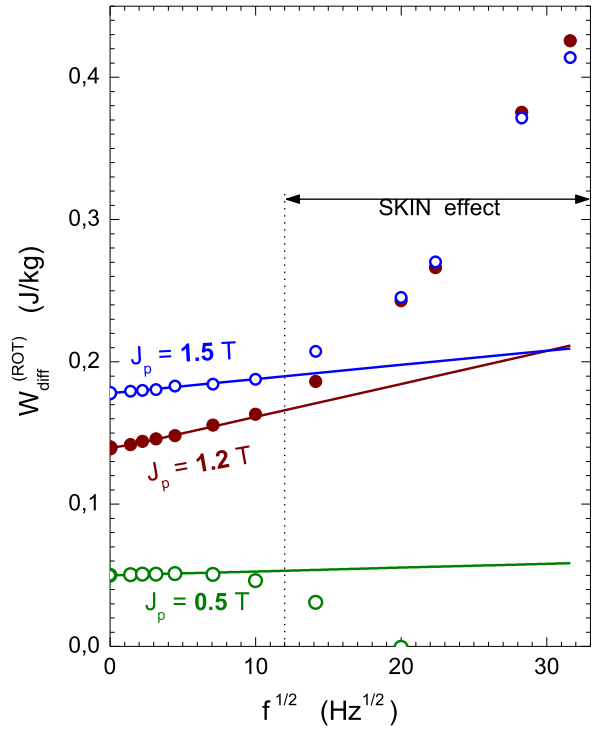

Fig. 16. Quantity $W_{\text{diff}}^{(\text{ROT})}(f) = W^{(\text{ROT})}(f) - W_{\text{class}}^{(\text{ROT})}(f)$, with $W_{\text{class}}^{(\text{ROT})}(f)$ calculated through the classical loss (10) corresponding to full flux penetration, is represented versus $f^{1/2}$. The rise of the skin effect beyond about 100 Hz is signaled by a sharp deviation (either upward or downward, depending on J_p) of $W_{\text{class}}^{(\text{ROT})}(f)$ from the STL predicted linear dependence on $f^{1/2}$ [50].

And subtract it from the measured loss, to obtain $W_{\text{diff}}^{(\text{ROT})}(f) = W^{(\text{ROT})}(f) - W_{\text{class}}^{(\text{ROT})}(f)$. This quantity is plotted as a function of $f^{1/2}$ in Fig. 16 [50]. We know by experiments that $W_{\text{diff}}^{(\text{ROT})}(f)$ measured in 0.30–0.20 mm thick

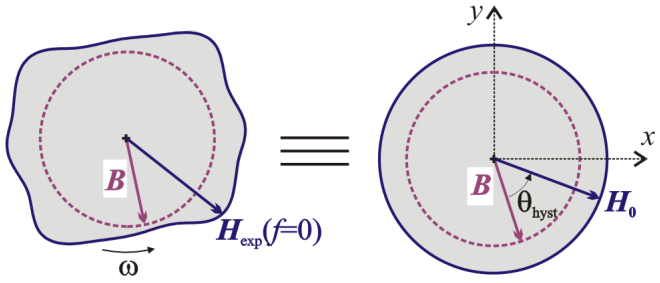

Fig. 17. $\boldsymbol{B}(\boldsymbol{H})$ magnetic constitutive law of a real material is assimilated, for imposed circular induction locus, to that of a perfectly isotropic material having the same static energy loss at the same induction [50]. $\boldsymbol{B}$ lags behind $\boldsymbol{H}_0$ by the angle θ_{hyst}.

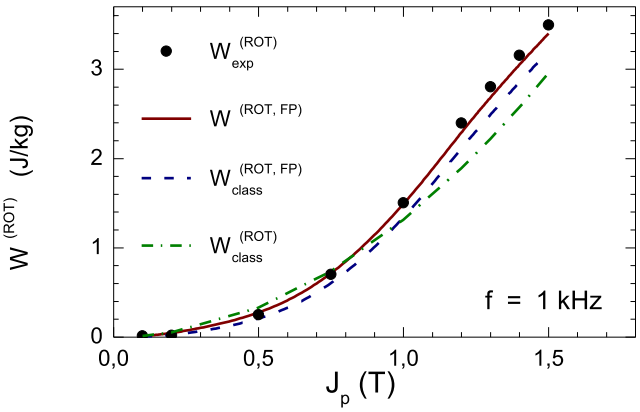

Fig. 18. Classical rotational loss component $W_{\text{class}}^{(\text{ROT})}(J_p)$ calculated at 1 kHz by (10) (no skin effect assumed, dash-dotted line) and by treating the skin effect through the FP method (dashed line). The latter method leads to the prediction of the total loss $W^{(\text{ROT,FP})}$(solid line). The symbols represent the experimental rotational loss [50].

laminations follows an $f^{1/2}$ dependence on frequency up to about 1 kHz [51]. Strong deviation from such a law of the quantity $W_{\text{diff}}^{(\text{ROT})}$ given by (10) is instead observed beyond about 100 Hz. It is caused by the surge of the skin effect, making the estimation of $W_{\text{class}}^{(\text{ROT})}(f)$ through (10) acceptable at low frequencies only.

A solution to this problem from the modeling viewpoint has been proposed in [50]. The material magnetic constitutive law is approximated by a $\boldsymbol{B}(\boldsymbol{H})$ vector constitutive law, identified at low frequencies, where magnetic isotropy is assumed. To this end, the real slightly anisotropic material is assimilated to the isotropic model material having the same hysteresis loss (see Fig. 17). The hysteresis contribution is therefore lumped, at any B_p level, in the phase delay θ_{hyst} of the vector $\boldsymbol{B}$ with respect to the rotating field vector of equivalent value $\boldsymbol{H_0}$. Both $\boldsymbol{B}$ and $\boldsymbol{H_0}$ have a constant modulus. This simplified constitutive law, decomposed along two orthogonal directions (x- and y-axes), is used in the diffusion (6), solved using the fixed point (FP) method [50]. The correspondingly calculated rotational loss prediction $W^{(\text{ROT,FP})}(J_p, f)$ at 1 kHz (a frequency for which skin effect is important) is shown versus J_p in Fig. 18. By (10) we overestimate the loss at low inductions, where the skin effect is linear and the factor F_{class} [see (2)] is always smaller than unity. The opposite occurs at high inductions, an effect engendered by the material non-linearity and the incipient saturation about the sheet surface. Note in this specific case that the combination of small

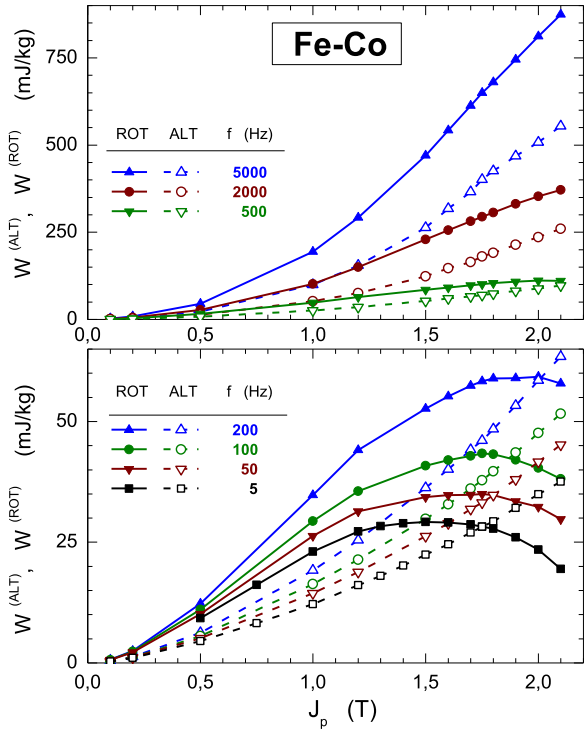

Fig. 19. Alternating and rotational energy losses are measured up to $J_p = 2.1$ T in 0.20 mm thick Fe–Co sheets [52].

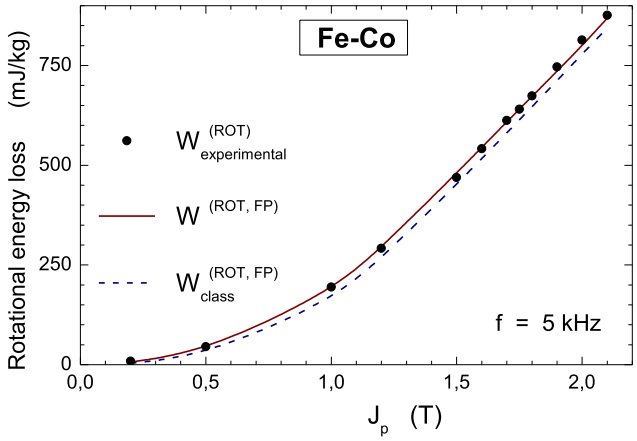

Fig. 20. Rotational loss measured versus polarization J_p at 5 kHz in a 0.20 mm thick Fe–Co sheet is predicted through loss decomposition and application of the FP method [52].

grain size and relevant sample thickness and conductivity makes the excess loss irrelevant. Consequently, the measured loss is well predicted as $W^{(\mathrm{ROT})}(J_p) = W_{\mathrm{hyst}}^{(\mathrm{ROT,FP})}(J_p) + W_{\mathrm{class}}^{(\mathrm{ROT,FP})}(J_p)$, where the hysteresis component is found by integrating, according to (5), the local $W_{\mathrm{hyst}}^{(\mathrm{ROT})}(J_p(x))$ along the calculated $J_p(x)$ profile.

B. 0.20 mm Thick Fe–Si and Fe–Co Laminations

Thin Fe-(3.2 wt.%)Si and Fe–Co samples have been investigated under alternating and circular loci in [52] in the range 5 Hz to 5 kHz. Fig. 19 provides the matrix of the measured energy loss figures versus frequency and peak polarization in a 0.20 mm thick Fe–Co sheet. Again, a predictive approach based on the diffusion equation coupled to the equivalent isotropic hysteresis constitutive law is followed. Fig. 20 shows a comparison between the calculated and measured $W^{(\mathrm{ROT})}(J_p)$ at 5 kHz in the range 0.20 T $\leq J_p \leq$ 2.1 T.

VI. Conclusion

High frequencies are ubiquitous in modern electrical applications and incomplete flux penetration in the magnetic core of machines and devices can occur. It is a troublesome effect, impairing the core efficiency and making arduous the assessment of the core behavior. This justifies research efforts toward better understanding and modeling of the skin effect in soft magnetic sheets, in connection with advanced measuring techniques. In this review, we summarize methods and results aimed at the improved knowledge of and predicting capability on the high-frequency performance, namely energy losses, of modern industrial products. The main emphasis is placed on the progress made in the authors' laboratories. A wide matrix of frequencies and induction levels is considered for (NO and HGO) Fe–Si and thin Fe–Co sheets, whose high-frequency loss behavior is measured and modeled. The discussion amply relies on the concept of loss decomposition and its extension to high frequencies. This feat is made non-trivial by the skin effect, especially when one must deal with the non-linear response of the material. The chosen examples actually run from relatively simple circumstances where low induction regimes are involved and linear approximations can be reasonably assumed to conditions where strongly non-linear magnetic constitutive equations must be accounted for. It is concluded that with the careful choice of simplifying assumptions, under the guidelines provided by the STL, a general framework of interpretation of the energy losses in magnetic sheets encompassing a range of frequencies eventually conducive to the skin effect can be worked out.

Acknowledgment

This work was supported in part by the 19ENG06 HEFMAG Project, which was funded through the EMPIR Program; and in part by the Co-Financed by the Participating States and the European Union's Horizon 2020 Research and Innovation Program.

References

[1] Y. Liu, C. Liu, X. Gao, and Y. Xiao, "Novel output regulation method for three-phase three-level wireless EV charging system," *IEEE Trans. Magn.*, vol. 58, no. 2, pp. 1–7, Feb. 2022.

[2] V. Basso et al., "Power losses in magnetic laminations with hysteresis: Finite element modeling and experimental validation," *J. Appl. Phys.*, vol. 81, no. 18, pp. 5606–5608, 1997.

[3] C. Ragusa, H. Zhao, C. Appino, M. Khan, O. de la Barrière, and F. Fiorillo, "Loss decomposition in non-oriented steel sheets: The role of the classical losses," *IEEE Magn. Lett.*, vol. 7, pp. 1–5, Aug. 2016.

[4] C. Beatrice, C. Appino, O. de la Barrière, F. Fiorillo, and C. Ragusa, "Broadband magnetic losses in Fe–Si and Fe–Co laminations," *IEEE Trans. Magn.*, vol. 50, no. 4, pp. 1–4, Apr. 2014.

[5] H. Zhao, C. Ragusa, O. de la Barrière, M. Khan, C. Appino, and F. Fiorillo, "Magnetic loss versus frequency in non-oriented steel sheets and its prediction: Minor loops, PWM, and the limits of the analytical approach," *IEEE Trans. Magn.*, vol. 53, no. 111, pp. 1–4, May 2017.

[6] D. Han, C. T. Morris, and B. Sarlioglu, "Common-mode voltage cancellation in PWM motor drives with balanced inverter topology," *IEEE Trans. Ind. Electron.*, vol. 64, no. 4, pp. 2683–2688, Apr. 2017.

[7] S. Takajo, T. Ito, T. Omura, and S. Okabe, "Loss and noise analysis of transformer ComprisingGrooved grain-oriented silicon steel," *IEEE Trans. Magn.*, vol. 53, no. 19, pp. 1–6, May 2017.

[8] R. Zeinali, D. Krop, and E. Lomonova, "Anisotropic congruency-based vector hysteresis model applied to non-oriented laminated steels," *IEEE Trans. Magn.*, vol. 57, no. 6, pp. 1–4, Jun. 2021.

[9] P. C. Sarker, Y. Guo, H. Y. Lu, and J. G. Zhu, "Measurement and modeling of rotational core loss of fe-based amorphous magnetic material under 2-D magnetic excitation," *IEEE Trans. Magn.*, vol. 57, no. 11, pp. 1–8, Nov. 2021.

[10] W. Yu, K. Liu, W. Hua, M. Hu, Z. Zhang, and J. Hu, "A new high-speed dual-stator flux switching permanent magnet machine with distributed winding," *IEEE Trans. Magn.*, vol. 58, no. 2, pp. 1–6, Feb. 2022.

[11] O. Messal et al., "Analysis of the dynamic behavior of magnetic materials under high B and dB/dt," in *Proc. Soft Magn. Materials Conf.*, 2017. [Online]. Available: https://hal.science/hal-01589353/

[12] B. Ducharne, P. Tsafack, Y. T. Deffo, B. Zhang, and G. Sebald, "Fractional operators for the magnetic dynamic behavior of ferromagnetic specimens: An overview," *AIP Adv.*, vol. 11, no. 13, p. 035309, 2021.

[13] D. M. Ionel, M. Popescu, S. J. Dellinger, T. J. E. Miller, R. J. Heideman, and M. I. McGilp, "On the variation with flux and frequency of the core loss coefficients in electrical machines," *IEEE Trans. Ind. Appl.*, vol. 42, no. 3, pp. 658–667, May 2006.

[14] Y. Chen and P. Pillay, "An improved formula for lamination core loss calculations in machines operating with high frequency and high flux density excitation," in *Proc. Conf. Rec. IEEE Ind. Appl. Conf., 37th IAS Annu. Meeting*, 2002, pp. 759–766.

[15] G. Bertotti, "General properties of power losses in soft ferromagnetic materials," *IEEE Trans. Magn.*, vol. 24, no. 11, pp. 621–630, Jan. 1988.

[16] M. Taghizadeh Kakhki, J. Cros, and P. Viarouge, "New approach for accurate prediction of eddy current losses in laminated material in the presence of skin effect with 2-D FEA," *IEEE Trans. Magn.*, vol. 52, no. 3, pp. 1–4, Mar. 2016.

[17] A.-T. Vo, M. Fassenet, V. Préault, C. Espanet, and A. Kedous-Lebouc, "New formulation of loss-surface model for accurate iron loss modeling at extreme flux density and flux variation: Experimental analysis and test on a high-speed PMSM," *J. Magn. Magn. Mater.*, vol. 563, Dec. 2022, Art. no. 169935.

[18] S. Hamada, F. Z. Louai, N. Nait-Said, and A. Benabou, "Dynamic hysteresis modeling including skin effect using diffusion equation model," *J. Magn. Magn. Mater.*, vol. 410, pp. 137–143, Jul. 2016.

[19] L. A. Pipes, "Matrix theory of skin effect in laminations," *J. Franklin Inst.*, vol. 262, no. 2, pp. 127–138, Aug. 1956.

[20] A. Boglietti, A. Cavagnino, M. Lazzari, and M. Pastorelli, "Predicting iron losses in soft magnetic materials with arbitrary voltage supply: An engineering approach," *IEEE Trans. Magn.*, vol. 39, no. 2, pp. 981–989, Mar. 2003.

[21] A. Boglietti, A. Cavagnino, M. Lazzari, and M. Pastorelli, "Two simplified methods for the iron losses prediction in soft magnetic materials supplied by PWM inverter," in *Proc. IEEE Int. Electric Mach. Drives Conf. (IEMDC)*, Jun. 2001, pp. 391–395.

[22] G. Grandi, M. K. Kazimierczuk, A. Massarini, U. Reggiani, and G. Sancineto, "Model of laminated iron-core inductors for high frequencies," *IEEE Trans. Magn.*, vol. 40, no. 4, pp. 1839–1845, Jul. 2004.

[23] L. Krahenbuhl, P. Dular, T. Zeidan, and F. Buret, "Homogenization of lamination stacks in linear magnetodynamics," *IEEE Trans. Magn.*, vol. 40, no. 2, pp. 912–915, Mar. 2004.

[24] P. Dular, J. Gyselinck, C. Geuzaine, N. Sadowski, and J. P. A. Bastos, "A 3-D magnetic vector potential formulation taking eddy currents in lamination stacks into account," *IEEE Trans. Magn.*, vol. 39, no. 13, pp. 1424–1427, May 2003.

[25] J. Gyselinck, L. Vandevelde, J. Melkebeek, P. Dular, F. Henrotte, and W. Legros, "Calculation of eddy currents and associated losses in electrical steel laminations," *IEEE Trans. Magn.*, vol. 35, no. 13, pp. 1191–1194, May 1999.

[26] H. Hamzehbahmani, P. Anderson, J. Hall, and D. Fox, "Eddy current loss estimation of edge burr-affected magnetic laminations based on equivalent electrical network—Part I: Fundamental concepts and FEM modeling," *IEEE Trans. Power Del.*, vol. 29, no. 2, pp. 642–650, Apr. 2014.

[27] Y. Zhang, P. Pillay, M. Ibrahim, and M. C. Cheng, "Magnetic characteristics and core losses in machine laminations: High-frequency loss prediction from low-frequency measurements," *IEEE Trans. Ind. Appl.*, vol. 48, no. 2, pp. 623–629, Mar. 2012.

[28] M. Ibrahim and P. Pillay, "Core loss prediction in electrical machine laminations considering skin effect and minor hysteresis loops," *IEEE Trans. Ind. Appl.*, vol. 49, no. 5, pp. 2061–2068, Sep. 2013.

[29] D. Roger, E. Napieralska-Juszczak, and A. Henneton, "High frequency extension of non-linear models of laminated cores," *COMPEL-Int. J. Comput. Math. Elect. Electron. Eng.*, vol. 25 no. 1, pp. 140–156, 2006.

[30] J. Gyselinck, R. V. Sabariego, and P. Dular, "A nonlinear time-domain homogenization technique for laminated iron cores in three-dimensional finite-element models," *IEEE Trans. Magn.*, vol. 42, no. 4, pp. 763–766, Apr. 2006.

[31] L. Dupre, O. Bottauscio, M. Chiampi, M. Repetto, and J. Melkebeek, "Modeling of electromagnetic phenomena in soft magnetic materials under unidirectional time periodic flux excitations," *IEEE Trans. Magn.*, vol. 35, no. 15, pp. 4171–4184, Sep. 1999.

[32] C. Appino et al., "Power losses in thick steel laminations with hysteresis," *J. Appl. Phys.*, vol. 79, no. 18, pp. 4575–4577, 1996.

[33] A. J. Bergqvist and S. G. Engdahl, "A homogenization procedure of field quantities in laminated electric steel," *IEEE Trans. Magn.*, vol. 37, no. 5, pp. 3329–3331, Sep. 2001.

[34] J. H. Krah, A. Bergqvist, and G. Engdahl, "Homogenization algorithms for calculation of field quantities in laminated magnetic materials," *IEEE Trans. Magn.*, vol. 38, no. 5, pp. 2385–2387, Sep. 2002.

[35] O. Bottauscio and M. Chiampi, "Laminated core modeling under rotational excitations including eddy currents and hysteresis," *J. Appl. Phys.*, vol. 89, no. 111, pp. 6728–6730, 2001.

[36] E. Dlala, O. Bottauscio, M. Chiampi, M. Zucca, A. Belahcen, and A. Arkkio, "Numerical investigation of the effects of loading and slot harmonics on the core losses of induction machines," *IEEE Trans. Magn.*, vol. 48, no. 12, pp. 1063–1066, Jan. 2012.

[37] P. Rasilo, E. Dlala, K. Fonteyn, J. Pippuri, A. Belahcen, and A. Arkkio, "Model of laminated ferromagnetic cores for loss prediction in electrical machines," *IET Electr. Power Appl.*, vol. 5, no. 17, pp. 580–588, 2011.

[38] S. E. Zirka, Y. I. Moroz, P. Marketos, A. J. Moses, D. C. Jiles, and T. Matsuo, "Generalization of the classical method for calculating dynamic hysteresis loops in grain-oriented electrical steels," *IEEE Trans. Magn.*, vol. 44, no. 9, pp. 2113–2126, Sep. 2008.

[39] A. Magni, C. Beatrice, O. Bottauscio, A. Caprile, E. Ferrara, and F. Fiorillo, "Magnetization process in thin laminations up to 1 GHz," *IEEE Trans. Magn.*, vol. 48, no. 14, pp. 1363–1366, Mar. 2012.

[40] A. Magni, O. Bottauscio, A. Caprile, F. Celegato, E. Ferrara, and F. Fiorillo, "Spin precession by pulsed inductive magnetometry in thin amorphous plates," *J. Appl. Phys.*, vol. 115, no. 117, p. 14A338, 2014.

[41] A. Magni, F. Fiorillo, E. Ferrara, A. Caprile, O. Bottauscio, and C. Beatrice, "Domain wall processes, rotations, and high-frequency losses in thin laminations," *IEEE Trans. Magn.*, vol. 48, no. 11, pp. 3796–3799, Nov. 2012.

[42] C. Beatrice et al., "Broadband magnetic losses of nanocrystalline ribbons and powder cores," *J. Magn. Magn. Mater.*, vol. 420, pp. 317–323, Dec. 2016.

[43] I. Mayergoyz, *Mathematical Models of Hysteresis*. Berlin, Germany: Springer, 1991.

[44] O. de la Barrière, C. Ragusa, C. Appino, F. Fiorillo, M. LoBue, and F. Mazaleyrat, "A computationally effective dynamic hysteresis model taking into account skin effect in magnetic laminations," *Phys. B, Condens. Matter*, vol. 435, pp. 80–83, Feb. 2014.

[45] A. Magni et al., "Domain structure and energy losses up to 10 kHz in grain-oriented Fe-Si sheets," *AIP Adv.*, vol. 11, no. 11, p. 015220, 2021.

[46] O. de la Barrière et al., "Wideband magnetic losses and their interpretation in HGO steel sheets," *J. Magn. Magn. Mater.*, vol. 565, p. 170214, 2023.

[47] G. Bertotti, *Hysteresis in Magnetism: For Physicists, Materials Scientists, and Engineers*. San Diego, CA, USA: Academic, 1998.

[48] F. Appino, C. Fiorillo, and C. Ragusa, "Loss decomposition under two-dimensional flux loci in non-oriented steel sheets," *Przeglad Elektrotechniczny*, vol. 83, no. 4, pp. 25–30, 2007.

[49] L'. Dáková et al., "Analysis of magnetic losses and complex permeability in novel soft magnetic composite with ferrite nanofibers," *IEEE Trans. Magn.*, vol. 54, no. 12, pp. 1–6, Dec. 2018.

[50] C. Appino et al., "Skin effect in steel sheets under rotating induction," *Int. J. Appl. Electromagn. Mech.*, vol. 48, pp. 247–254, 2015.

[51] O. de la Barrière, C. Appino, F. Fiorillo, M. Lécrivain, C. Ragusa, and P. Vallade, "A novel magnetizer for 2D broadband characterization of steel sheets and soft magnetic composites," *Int. J. Appl. Electromagn. Mech.*, vol. 48, pp. 239–245, 2015.

[52] C. Appino, O. de la Barriere, C. Beatrice, F. Fiorillo, and C. Ragusa, "Rotational magnetic losses in non-oriented Fe-Si and Fe-Co laminations up to the kHz range," *IEEE Trans. Magn.*, vol. 50, no. 111, pp. 1–4, Nov. 2014.